Supporting Information

1 Measurements of cyclic voltammetry (CV) and electrochemical impedance spectroscopy (EIS) curves

1) CV measurement conditions for the MnO_x/Ti flow-through anode

The scanning electrolyte solution was 7 g/L Na_2SO_4 with and without 600 mg/L AO7 at a scan rate of 10 mV/s.

2) CV measurement conditions for the biofilm-attached carbon felts

The reactor used for CV measurements consisted of an anode chamber (3 cm × 3 cm × 2 cm) and a cathode chamber (3 cm × 3 cm × 2 cm) separated by a cation exchange membrane (CEM, project area of 3 cm × 3 cm). The cathode chamber with an inserted saturated calomel electrode was filled with the biofilm-attached carbon felts. The Pt counter electrode was inserted into the anode chamber. The electrolyte solution in the anode chamber was 7 g/L Na_2SO_4 and 600 mg/L AO7. Four types of electrolyte solutions were scanned in the cathode chamber, including the cathode influent, the nutrient solution, 600 mg/L AO7 solution, and 300 mg/L AO7 solution. Specifically, the cathode influent was prepared by mixing the anode effluent (obtained under the current of 6 mA, the flow rate of 0.25 mL/min, and the feed AO7 concentration of 600mg/L) with 3.4 g/L KH_2PO_4, 5.7 g/L $K_2HPO_4{\cdot}3H_2O$, and 0.44 g/L NH_4Cl. The nutrient solution contained 3.4 g/L KH_2PO_4, 5.7 g/L $K_2HPO_4{\cdot}3H_2O$, and 0.44 g/L NH_4Cl in deionized (DI) water. The 600 or 300 mg/L AO7 solutions were prepared by mixing 600 or 300 mg/L AO7 with 3.4 g/L KH_2PO_4, 5.7 g/L $K_2HPO_4{\cdot}3H_2O$, and 0.44 g/L NH_4Cl in DI water. The four types of electrolyte solutions were aerated in a bottle and recirculated between the bottle and the cathode chamber during measurements. The cathode influent was aerated with N_2 or air while the other three electrolyte solutions were aerated with only air. The scan rate was 1 mV/s and the scan range was –1.2–0 V vs. SCE.

3) EIS measurement conditions for the biofilm-attached carbon felts and pristine carbon felts

The reactor used for EIS measurements was the same as that used in the CV measurements for the biofilm-attached carbon felts as described above. The electrolyte solution in the anode chamber was 7 g/L Na_2SO_4 and 600 mg/L AO7. The electrolyte solution in the cathode chamber was prepared by mixing the anode effluent (obtained under the current of 6 mA, the flow rate of 0.25 mL/min, and the feed AO7 concentration of 600 mg/L) with 3.4 g/L KH_2PO_4, 5.7 g/L $K_2HPO_4{\cdot}3H_2O$, and 0.44 g/L NH_4Cl. The frequency range was 0.001–10^6 Hz and the scan rate was 5 mV/s at the open circuit condition.

2 Calculation of COD and AO7 removal efficiencies

1) During the startup period of the electrocatalytic biofilm reactor (ECBR)

During the startup period of the ECBR, the anodic ($R_{a,\ COD}$), cathodic ($R_{c,\ COD}$), and total ($R_{t,\ COD}$) COD removal efficiencies were calculated using Eqs. (S1)–(S3).

$$R_{a,\ COD}=\frac{COD_{a,\ influent}-COD_{a,\ effluent}}{COD_{a,\ influent}} \quad , \qquad (S1)$$

where $COD_{a,\ influent}$ and $COD_{a,\ effluent}$ are the COD concentrations in the anode influent and effluent bottles (mg/L), respectively.

$$R_{c,\ COD}=\frac{COD_0-COD_t}{COD_0} \quad , \qquad (S2)$$

where COD_0 is the initial value of COD concentration (mg/L) in the cathode circulation bottle; COD_t is the COD concentration (mg/L) in the cathode circulation bottle on the day t.

$$R_{t,\ COD}=\frac{COD_{a,\ influent}-COD_{c,4}}{COD_{a,\ influent}} \quad , \qquad (S3)$$

where $COD_{a,\ influent}$ is the COD concentration in the anode influent bottle (mg/L); $COD_{c,4}$ is the COD concentration in the cathode circulation bottle on the 4th day of every cycle (mg/L).

2) During the continuous operation period of ECBR

During the continuous operation period of ECBR, the anodic ($R_{a,\ COD}$), cathodic ($R_{c,\ COD}$), and total ($R_{t,\ COD}$) COD removal efficiencies were calculated using Eqs. (S4)–(S6).

$$R_{a,\ COD}=\frac{COD_{a,\ influent}-COD_{a,\ effluent}}{COD_{a,\ influent}} \quad , \qquad (S4)$$

where $COD_{a,\ influent}$ and $COD_{a,\ effluent}$ are the COD concentrations in the anode influent and effluent bottles (mg/L), respectively.

$$R_{c,\ COD}=\frac{COD_{a,\ effluent}-COD_{c,\ effluent}}{COD_{a,\ effluent}} \quad , \qquad (S5)$$

where $COD_{a,\ effluent}$ and $COD_{c,\ effluent}$ are the COD concentrations in anode and cathode effluent bottles (mg/L), respectively.

$$R_{t,\ COD}=\frac{COD_{a,\ influent}-COD_{c,effluent}}{COD_{a,\ influent}} \quad , \qquad (S6)$$

where $COD_{a,\ influent}$ and $COD_{c,\ effluent}$ are the COD concentrations (mg/L) in anode influent and cathode effluent bottles, respectively.

AO7 removal efficiency in the ECBR was calculated using Eq. (S7).

$$R_{\mathrm{ECBR,\ AO7}}=\frac{\mathrm{AO7_{a,\ influent}}-\mathrm{AO7_{c,\ effluent}}}{\mathrm{AO7_{a,\ influent}}}\quad , \qquad \text{(S7)}$$

where $\mathrm{AO7_{a,\ influent}}$ and $\mathrm{AO7_{c,\ effluent}}$ are the AO7 concentrations (mg/L) in the anode influent and cathode effluent bottles, respectively.

3) For the electrocatalytic reactor-stainless steel mesh cathode (ECR-SS) and biofilm reactor (BR)

COD removal efficiencies of ECR-SS and BR were calculated using Eq. (S8).

$$R_{\mathrm{COD}}=\frac{\mathrm{COD_{Influent}}-\mathrm{COD_{Effluent}}}{\mathrm{COD_{Influent}}}\quad , \qquad \text{(S8)}$$

where $\mathrm{COD_{Influent}}$ and $\mathrm{COD_{Effluent}}$ are the COD concentrations (mg/L) in the influent and effluent bottles, respectively.

AO7 removal efficiencies of the ECR-SS and BR were calculated using Eq. (S9).

$$R_{\mathrm{AO7}}=\frac{\mathrm{AO7_{Influent}}-\mathrm{AO7_{Effluent}}}{\mathrm{AO7_{Influent}}}\quad , \qquad \text{(S9)}$$

where $\mathrm{AO7_{Influent}}$ and $\mathrm{AO7_{Effluent}}$ are the AO7 concentrations (mg/L) in the influent and effluent bottles, respectively.

3 Calculation of energy consumption

The energy consumption (EC, kWh/kg COD) of ECBR and ECR-SS was calculated using Eq. (S10) (Moreira et al., 2017).

$$\mathrm{EC}=\frac{UI}{1000Q\ (\mathrm{COD_{Influent}}\text{-}\mathrm{COD_{Effluent}})}\quad , \qquad \text{(S10)}$$

where U is the applied voltage (V), I is the applied current (A), Q is the treated flow rate (L/h). For ECBR, $\mathrm{COD_{Influent}}$ and $\mathrm{COD_{Effluent}}$ are the COD concentrations (kg/L) in the anode influent and cathode effluent bottles, respectively. For ECR-SS, $\mathrm{COD_{Influent}}$ and $\mathrm{COD_{Effluent}}$ are the COD concentrations (kg/L) in the influent and effluent bottles, respectively.

4 Analysis of intermediate products of AO7

The intermediate products of AO7 were detected using the gas chromatography-mass spectrometry (GC-MS, QP2020NX, Shimadzu, Japan). The samples were subjected to the solid phase extraction

before the GC-MS analysis. The solid phase extraction included the following three steps: 1) 10 mL methanol and 10 mL ultrapure water were used to activate the Waters Max-C18 column (Waters, USA); 2) 100 mL sample was sucked through Waters Max-C18 at a flow rate of 4 mL under vacuum and then was eluted using methanol; 3) The eluate was concentrated by the termovap sample concentrator and saved to a 1.5 mL sample bottle. GC-MS measurements were performed with the SH-Rxi-5Sil MS column (30 m × 0.25 mm × 0.25 μm; Shimadzu, Japan). The column temperature program was as follows (Cao et al., 2017): the temperature was hold at 50℃ for 2 min, increased to 250℃ at 10℃/min, hold at 250℃ for 1 min, increased to 300℃ at 5℃/min, and hold at 300℃ for 2 min. The temperatures of the interface source and the ion source were 280℃ and 220℃, respectively. The electron energy of electron ionization was 70 eV and the scan range was from 40 to 700 m/z.

The intermediate products of AO7 were also analyzed with the high performance liquid chromatography-mass spectrometry (HPLC-MS, 1290-qtof6550, Agilent, USA) equipped with a C18 column (Waters BE, USA; 2.1 mm × 50 mm × 1.7 μm). The mobile phase was the mixture of methanol and ultrapure water at a flow rate of 0.3 mL/min. The gradient elution was used and the elution procedure was shown in Table S1. The injected volume of samples was 2 μL. MS used the negative ion modes. In the negative ion mode, the voltage was 3200 kV; the sphericular gas temperature was 350℃; the flow rate of sphericular gas was 12 L/min. The M/Z range was 20–600.

5 Analysis of hydroxylated products of salicylic acid (SA)

2,3-DHBA, 2,5-DHBA, and catechol, the three hydroxylated products produced by the reaction between SA and ·OH, were measured by the high performance liquid chromatography (HPLC, DGU-A20, Shimadzu, Japan) equipped with a C18 column (dimension of 4.6 mm × 250 mm, Shimadzu, Japan) and a UV-diode array detector (Fernández-Castro et al., 2015). Methanol/0.1% phosphoric acid (40:60, v/v) was used as the mobile phase at a flow rate of 0.7 mL/min and the column temperature was 40℃ (Mo et al., 2020). The wavelength for the detection of the three hydroxylated products and SA was 210 nm. The retention time of 2,3-DHBA, 2,5-DHBA, catechol, and SA was 23.001, 16.982, 15.616, and 42.381 min, respectively.

6 Calculation of current contributed by AO7 reduction

Current (*I*, A) contributed by AO7 reduction was calculated using Eq. (S11).

$$I=\frac{4\times Q\times AO7\times NA\times 1.602\times 10^{-19}}{350.34} \quad , \qquad \text{(S11)}$$

where Q is the treated flow rate (L/s); $AO7$ is the AO7 concentrations (g/L) in the cathode influent bottle; NA is avogadro constant (1/mol); 1.602×10^{-19} is the unit electric charge (C);

350.24 is the molar mass of AO7 (g/mol); 4 is electron number required by one AO7 molecule to be reduced (Eq. (S12)).

$$C_{16}H_{11}N_2O_4SNa+4H^++4e^-\rightarrow C_6H_6NSO_3Na+C_{10}H_9NO \quad (S12)$$

Table S1 The mobile phase gradient elution procedure for HPLC-MS.

Time (min)	Methanol (v/v, %)	H_2O (v/v, %)
0–10	90	10
10–15	90–10	10–90
15–20	10	90
20–21	10–90	90–10
21–22	90	10

Table S2 Comparison of the electrocatalytic biofilm reactor with the anodic oxidation process in removing azo dyes.

No.	Azo dye	Anode	COD Removal Efficiency (%)	EC[b)] (kWh/kg COD)	Reference
1	Acid Red G (100 mg/L)	PbO_2/Ti+Fe_3O_4/Sb-SnO_2 particles	65.89 (120 min) [a)]	1060	Yuan et al., 2019
2	Amaranth dye (100 mg/L)	Pt-SnSb/Ti	70.3 (360 min)	700	Fajardo et al., 2017
3	Acid Yellow 23 (100 mg/L)	Graphite	76 (20 min)	730	GilPavas et al., 2016
4	Mordant Blue 13 (200 mg/L)	IrO_2/RuO_2/Ti	79 (240 min)	113	Kenova et al., 2018
5	Acid Black 2 (Concentration unknown)	Boron-doped diamond	90 (99 min)	83.51	Wan et al., 2019
6	Acid Violet 7 (200 mg/L)	Boron-doped diamond	82.2 (120 min)	1180	Brito et al., 2018
7	Basic Red 13 (100 mg/L)	Pt/Ti	99.9 (Time unknown)	0.98	Ozturk and Yilmaz, 2020
8	Methyl Orange (65 mg/L)	β-$Ni(OH)_2$/Nickel foam	63.0 (180 min)	22.2	Sun et al., 2018

Notes: a) The time shown in the bracket is the electrolysis time; b) Energy consumption.

Table S3 Comparison of the electrocatalytic biofilm reactor with the bioelectrochemical systems (BESs) in removing azo dyes.

No.	Azo dye	BES	Co-substrate	COD Removal Efficiency (%)	Reference
1	Acid orange 7 (100 mg/L)	MEC[a)]	Glucose (Concentration unknown)	51.19	Wang et al., 2018
2	Acid orange 7 (100 mg/L)	MEC+BCO[b)]	Glucose (Concentration unknown)	89.12	Wang et al., 2018
3	Reactive brilliant red X-3B (200 mg/L)	BER[c)]	Glucose (250 mg/L)	82.9	Sun et al., 2022
4	New coccine (25 mg/L)	MFC[d)]	Sodium acetate (440 mg/L)	73	Oon et al., 2017
5	Acid orange 7 (200 mg/L)	Stacked MEC	Glucose (1000 mg/L)	50.9	Kong et al., 2018
6	Methyl orange (300 mg/L)	3D-EF[e)]-MFCs	Glucose (500 mg COD/L)	84.1	Sun et al., 2022
7	Reactive brilliant red X-3B (200 mg/L)	BER	Glucose (400 mg/L)	75.64	Cao et al., 2018
8	Cong red (700 mg/L)	MFC	Glucose (2500 mg/L)	73.96	Prajapati and Yelamarthi, 2020

Notes: a) Microbial electrolysis cell; b) Biocontact oxidation; c) Biofilm electrode reactor; d) Microbial fuel cell; e) Electro-Fenton.

Table S4 Intermediate products of AO7 in the electrocatalytic biofilm reactor analyzed by GC-MS and HPLC-MS.

Sample	Methods	Retention time (min)	Molecular formula	Product name	Product structure
Anode effluent	GC-MS	11.675	$C_8H_6O_4$	Phthalic acid	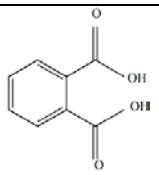
		12.14	$C_8H_6O_2$	Phthalate	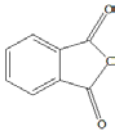
	HPLC-MS	1.804	$C_6H_4O_2$	Benzoquinone	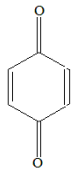
		2.345	$C_8H_6O_4$	Phthalic acid	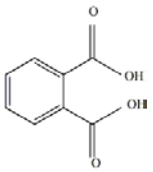
		4.28	$C_{10}H_8O$	1-naphthol	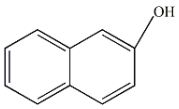
Cathode effluent	GC-MS	3.31	$C_6H_{14}O$	2-hexanol	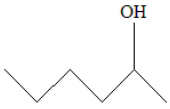
		6.94	$C_8H_{18}O$	2-propyl-1-pentanol	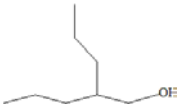

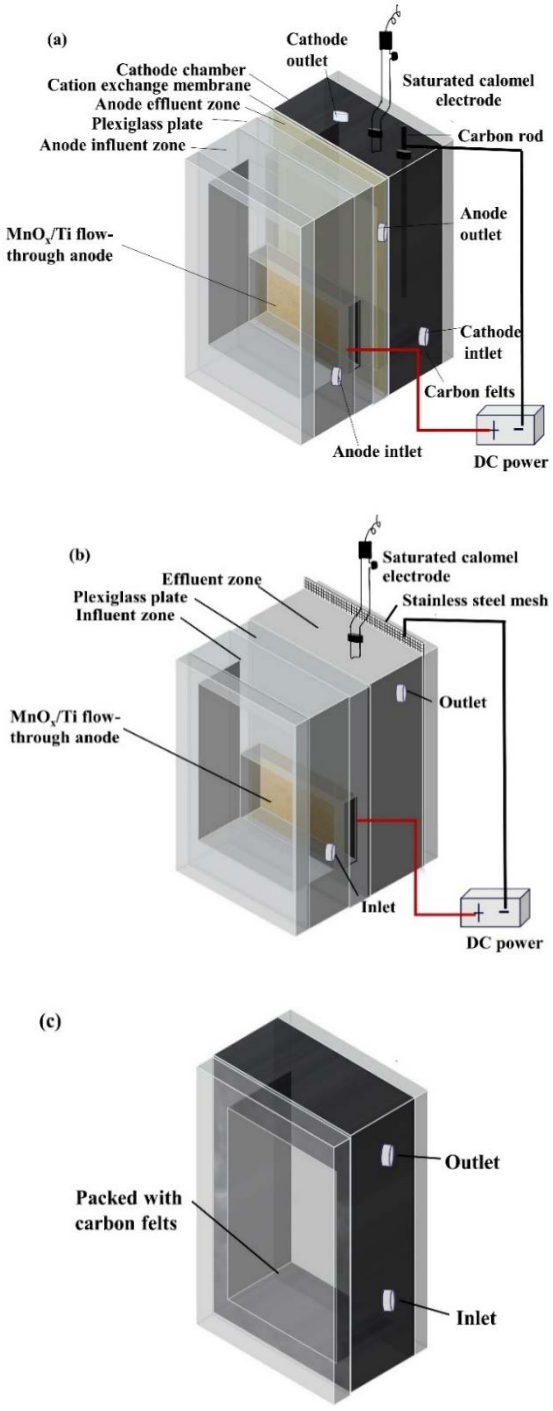

Fig. S1 Schematic diagrams of the electrocatalytic biofilm reactor (ECBR) (a), electrocatalytic reactor-stainless steel mesh cathode (ECR-SS) (b), and biofilm reactor (BR) (c).

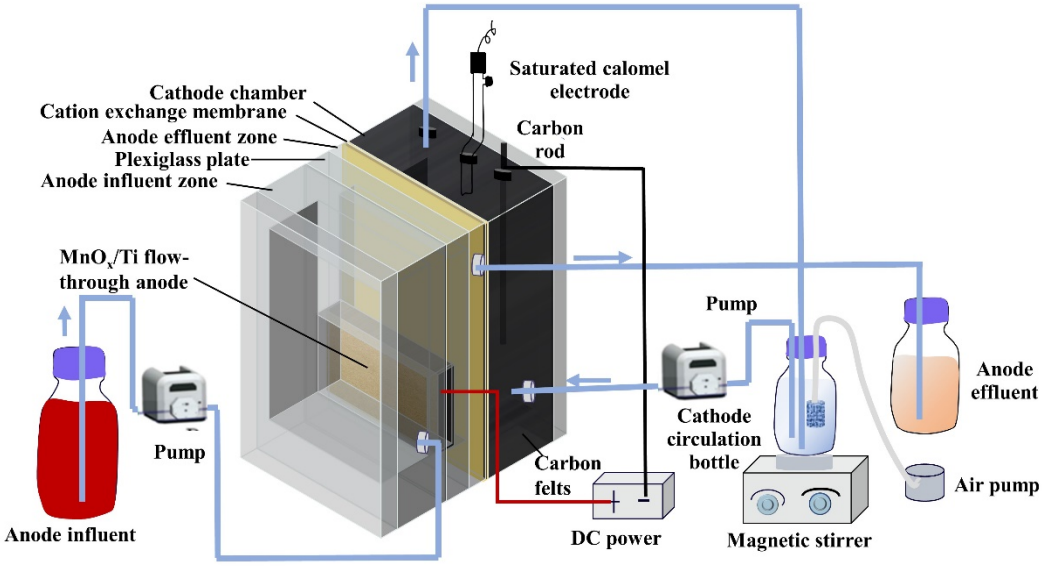

Fig. S2 Schematic diagram of the electrocatalytic biofilm reactor (ECBR) with the cathode chamber operated in the batch mode during the startup period.

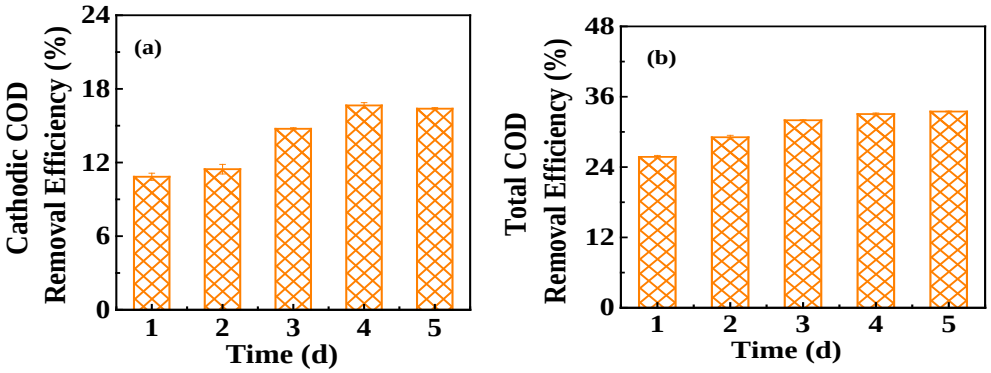

Fig. S3 The cathodic (a) and total COD removal efficiencies (b) after the operation mode of the electrocatalytic biofilm reactor (ECBR) was switched to the continuous mode.

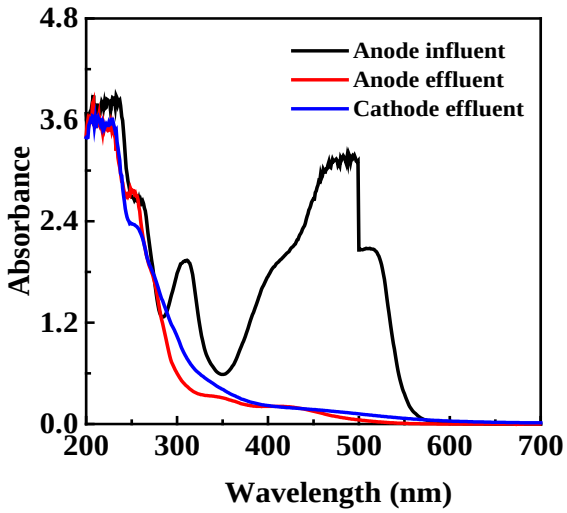

Fig. S4 UV-vis absorption spectra of the AO7 synthetic wastewater before (anode influent) and after (anode effluent and cathode effluent) treatment in the electrocatalytic biofilm reactor (ECBR). Operation conditions: the AO7 concentration was 600 mg/L; the current was 6 mA; the treated flow rate was 0.25 mL/min.

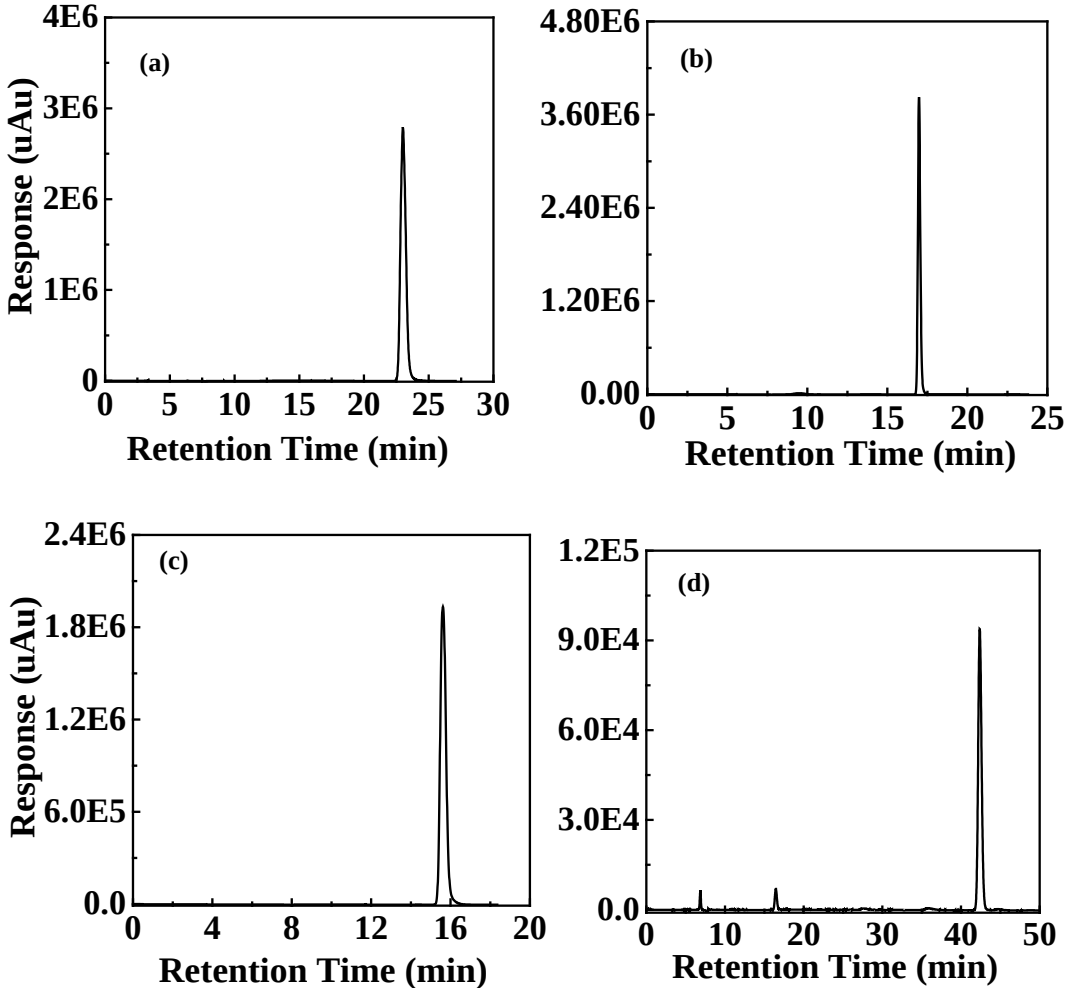

Fig. S5 High performance liquid chromatography of 2,3-DHBA (a), 2,5-DHBA (b), catechol (c), and salicylic acid (d). The retention time of 2,3-DHBA, 2,5-DHBA, catechol, and SA was 23.001, 16.982, 15.616, and 42.381 min, respectively.

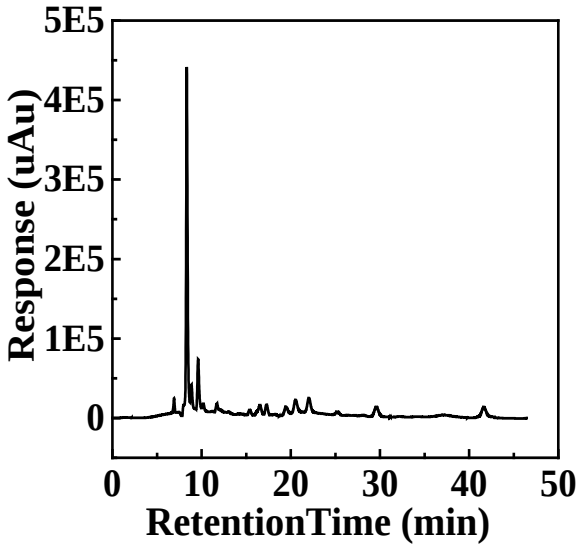

Fig. S6 High performance liquid chromatography analysis on the hydroxylated products of salicylic acid after treated in the anode chamber of the electrocatalytic biofilm reactor. The electrocatalytic biofilm reactor was operated under 6 mA. The anode influent contained 600 mg/L salicylic acid and 7 g/L Na_2SO_4 (pH was adjusted to 6.8).

References

Brito C N, Ferreira M B, de Moura Santos E C M, Léon J J L, Ganiyu S O, Martínez-Huitle C A (2018). Electrochemical degradation of azo-dye acid violet 7 using BDD anode: effect of flow reactor configuration on cell hydrodynamics and dye removal efficiency. Journal of Applied Electrochemistry, 48(12): 1321–1330

Cao X, Wang H, Zhang S, Nishimura O, Li X (2018). Azo dye degradation pathway and bacterial community structure in biofilm electrode reactors. Chemosphere, 208: 219–225

Cao Z, Zhang J, Zhang J, Zhang H (2017). Degradation pathway and mechanism of Reactive Brilliant Red X-3B in electro-assisted microbial system under anaerobic condition. Journal of Hazardous Materials, 329: 159–165

Fajardo A S, Martins R C, Silva D R, Quinta-Ferreira R M, Martinez-Huitle C A (2017). Electrochemical abatement of amaranth dye solutions using individual or an assembling of flow cells with Ti/Pt and Ti/Pt-SnSb anodes. Separation and Purification Technology, 179: 194–203

Fernández-Castro P, Vallejo M, San Román M F, Ortiz I (2015). Insight on the fundamentals of advanced oxidation processes. role and review of the determination methods of reactive oxygen species. Journal of Chemical Technology and Biotechnology (Oxford, Oxfordshire), 90(5): 796–820

GilPavas E, Dobrosz-Gomez I, Gomez-García M Á (2016). Electrochemical degradation of acid yellow 23 by anodic oxidation-optimization of operating parameters. Journal of Environmental Engineering, 142(11): 04016052

Kenova T A, Kornienko G V, Golubtsova O A, Kornienko V L, Maksimov N G (2018). Electrochemical degradation of Mordant Blue 13 azo dye using boron-doped diamond and dimensionally stable anodes: influence of experimental parameters and water matrix. Environmental Science and Pollution Research International, 25(30): 30425–30440

Kong F, Ren H, Pavlostathis S G, Wang A, Nan J, Ren N Q (2018). Enhanced azo dye decolorization and microbial community analysis in a stacked bioelectrochemical system. Chemical Engineering Journal, 354: 351–362

Mo Y, Du M, Yuan T, Liu M, Wang H, He B, Li J, Zhao X (2020). Enhanced anodic oxidation and energy saving for dye removal by integrating O2-reducing biocathode into electrocatalytic reactor. Chemosphere, 252: 126460

Moreira F C, Boaventura R A R, Brillas E, Vilar V J P (2017). Electrochemical advanced oxidation processes: a review on their application to synthetic and real wastewaters. Applied Catalysis B: Environmental, 202: 217–261

Oon Y S, Ong S A, Ho L N, Wong Y S, Oon Y L, Lehl H K, Thung W E, Nordin N (2017). Microbial fuel cell operation using monoazo and diazo dyes as terminal electron acceptor for simultaneous decolourisation and bioelectricity generation. Journal of Hazardous Materials, 325: 170–177

Ozturk D, Yilmaz A E (2020). Investigation of electrochemical degradation of basic red 13 dye in aqueous solutions based on COD removal: Numerical optimization approach. International Journal of Environmental Science and Technology, 17(5): 3099–3110

Prajapati S, Yelamarthi P S (2020). Microbial fuel cell-assisted congo red dye decolorization using biowaste-derived anode material. Asia-Pacific Journal of Chemical Engineering, 15(5): 1–10

Sun L, Mo Y, Zhang L (2022). A mini review on bio-electrochemical systems for the treatment of azo dye wastewater: State-of-the-art and future prospects. Chemophere, 294: 133801

Sun S, Diao P, Feng C, Ungureanu E M, Tang Y, Hu B, Hu Q (2018). Nickel-foam-supported β-Ni(OH)2 as a green anodic catalyst for energy efficient electrooxidative degradation of azo-dye wastewater. RSC Advances, 8(35): 19776–19785

Wan J, Liu B, Jin C, Li J L, Wei X, Dong H X, Xu Z Y, Gao M C, Zhao Y G (2019). Electrochemical oxidation of acid black 2 dye wastewater using boron-doped diamond anodes: Multiresponse optimization and degradation mechanisms. Environmental Engineering Science, 36(9): 1049–1060

Wang Y, Pan Y, Zhu T, Wang A, Lu Y, Lv L, Zhang K, Li Z (2018). Enhanced performance and microbial community analysis of bioelectrochemical system integrated with bio-contact oxidation reactor for treatment of wastewater containing azo dye. Science of the Total Environment, 634: 616–627

Yuan M, Salman N M, Guo H, Xu Z, Xu H, Yan W, Liao Z W, Wang Y (2019). A 2.5D electrode system constructed of magnetic Sb-SnO_2 particles and a PbO_2 electrode and its electrocatalysis application on acid red. Catalysts, 9(11): 875